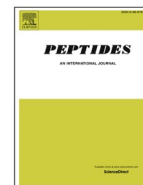




Since January 2020 Elsevier has created a COVID-19 resource centre with free information in English and Mandarin on the novel coronavirus COVID-19. The COVID-19 resource centre is hosted on Elsevier Connect, the company's public news and information website.

Elsevier hereby grants permission to make all its COVID-19-related research that is available on the COVID-19 resource centre - including this research content - immediately available in PubMed Central and other publicly funded repositories, such as the WHO COVID database with rights for unrestricted research re-use and analyses in any form or by any means with acknowledgement of the original source. These permissions are granted for free by Elsevier for as long as the COVID-19 resource centre remains active.



## An angiotensin-converting enzyme-2-derived heptapeptide GK-7 for SARS-CoV-2 spike blockade

Songling Han<sup>a,1</sup>, Gaomei Zhao<sup>a,1</sup>, Zhuanzhuan Wei<sup>a,1</sup>, Yin Chen<sup>a</sup>, Jianqi Zhao<sup>a</sup>, Yongwu He<sup>a</sup>, Ying-Juan He<sup>a</sup>, Jining Gao<sup>a</sup>, Shilei Chen<sup>a</sup>, Changhong Du<sup>a</sup>, Tao Wang<sup>a</sup>, Wei Sun<sup>b</sup>, Yi Huang<sup>b</sup>, Cheng Wang<sup>a,\*</sup>, Junping Wang<sup>a,\*</sup>

<sup>a</sup> State Key Laboratory of Trauma, Burns and Combined Injury, Institute of Combined Injury of PLA, Chongqing Engineering Research Center for Nanomedicine, College of Preventive Medicine, Third Military Medical University, Chongqing, 400038, China

<sup>b</sup> Biomedical Analysis Center, Third Military Medical University, Chongqing, 400038, China

### ARTICLE INFO

#### Keywords:

Antiviral peptide  
SARS-CoV-2  
Spike  
Receptor binding domain  
Angiotensin-converting enzyme-2

### ABSTRACT

The ongoing coronavirus disease 2019 (COVID-19) pandemic caused by severe acute respiratory syndrome coronavirus 2 (SARS-CoV-2) infection is a global concern and necessitates efficient drug antagonists. Angiotensin-converting enzyme-2 (ACE2) is the main receptor of SARS-CoV-2 spike 1 (S1), which mediates viral invasion into host cells. Herein, we designed and prepared short peptide inhibitors containing 4–6 critical residues of ACE2 that contribute to the interaction with SARS-CoV-2 S1. Among the candidates, a peptide termed GK-7 (GKGDFRI), which was designed by extracting residues ranging from Gly353 to Ile359 in the ligand-binding domain of ACE2, exhibited the highest binding affinity (25.1 nM) with the SARS-CoV-2 spike receptor-binding domain (RBD). GK-7 bound to the RBD and decreased SARS-CoV-2 S1 attachment to A549 human alveolar epithelial cells. Owing to spike blockade, GK-7 inhibited SARS-CoV-2 spike pseudovirus infection in a dose-dependent manner, with a half-maximal inhibitory concentration of 2.96 µg/mL. Inspiringly, pulmonary delivery of GK-7 by intranasal administration did not result in toxicity in mice. This study revealed an easy-to-produce peptide inhibitor for SARS-CoV-2 spike blockade, thus providing a promising candidate for COVID-19 treatment.

### 1. Introduction

Coronavirus disease 2019 (COVID-19) induced by severe acute respiratory syndrome coronavirus 2 (SARS-CoV-2) is a global concern and has caused more than 4,300,000 deaths worldwide [1]. Although contact and transplacental transmission have been reported for SARS-CoV-2 [2,3], the virus mainly invades humans through the respiratory tract [4]. Similar to the pathological manifestations of severe acute respiratory syndrome coronavirus (SARS-CoV) and Middle East respiratory syndrome coronavirus (MERS-CoV) that emerged in 2003 and 2012, respectively [5,6], diffuse alveolar damage and pulmonary hyaline membranes, which are characteristic of acute respiratory distress syndrome, are observed in the lungs of patients who die from COVID-19 [7]. It has been reported that respiratory failure, sepsis, and coagulation disorders are common lethal complications in COVID-19 patients [8].

The employment of inhibitors targeting the pathogenic processes of SARS-CoV-2, including membrane adhesion and fusion, virion uncoating, genome integration and replication, and viral assembly and release, is useful for COVID-19 treatment.

The association of the viral spike, which is composed of the two subunits spike 1 (S1) and 2, with sensitive cells through receptor-ligand interactions is the initial step in SARS-CoV-2 infection. S1 contains a receptor-binding domain (RBD) that mediates viral attachment [9]. Because the sequence of the SARS-CoV-2 spike is 76.47 % homologous to that of SARS-CoV [10], angiotensin-converting enzyme-2 (ACE2), which is the host receptor for SARS-CoV, is also considered a crucial cell target of SARS-CoV-2 [11]. Further studies have confirmed that the binding affinity of SARS-CoV-2 S1 for ACE2 is as low as 8.02 nM [12]. Additionally, cells insensitive to SARS-CoV-2 are attacked by the virus after ACE2 transfection [13]. Since ACE2 is abundant in alveolar epithelial

\* Corresponding authors.

E-mail addresses: [wangctmmu@126.com](mailto:wangctmmu@126.com) (C. Wang), [wangjunping@tmmu.edu.cn](mailto:wangjunping@tmmu.edu.cn) (J. Wang).

<sup>1</sup> These authors contribute equally to this study.

cells and enterocytes, the lung and intestine are susceptible to SARS-CoV-2 infection [14].

Lung infection generally initiates from SARS-CoV-2 colonization in the nasal cavity for several days [15], during which intranasal delivery of inhibitors is beneficial for suppressing viral invasion in the early stage. Recombinant receptor proteins are potential inhibitors of corresponding viruses [16]. Recombinant ACE2 has been confirmed to trap SARS-CoV-2 [17]. Nevertheless, similar to monoclonal antibodies developed for the systemic treatment of COVID-19 [18], ACE2 is a large protein that is not ideal for intranasal delivery not only due to difficulties in preparation and preservation but also due to the low density of binding sites [19]. Instead, ACE2-derived peptide inhibitors with high affinity for the SARS-CoV-2 spike are promising candidates for local medication [20,21].

The detailed structure of the SARS-CoV-2 spike RBD bound to ACE2 was resolved at 2.45 Å by X-ray crystal diffraction [22]. Herein, we designed and synthesized several short peptides based on the ligand-binding domain of ACE2. Among the candidates, a peptide termed GK-7 was screened by RBD binding analysis and spike blocking experiments. The antiviral action of GK-7 was evaluated using SARS-CoV-2 spike pseudovirions. Furthermore, the mechanism by which GK-7 blocks RBD binding was investigated by molecular dynamics simulation (MDS). This study aimed to identify an easy-to-produce peptide inhibitor for curbing SARS-CoV-2 infection and provide an alternative scheme for COVID-19 treatment.

## 2. Materials and methods

### 2.1. Peptide preparation

All peptides were fabricated by Guoping Pharmaceutical Company (Hefei, Anhui, China) using automatic solid-phase synthesis [23]. The prepared peptides were desalted using a strongly basic styrene-chlorine anion exchange resin (BASF, Tianjin, China) and were freeze-dried. The purities of the peptides were determined by high-performance liquid chromatography (SHIMADZU LC-10AT, Kyoto, Japan). Chromatographic data were acquired on a SHIMADZU Inertsil ODS-SP column (5 µm, 4.6 × 250 mm), applying a linear gradient of 15–55 % buffer B (buffer A: 0.1 % trifluoroacetic acid in water; buffer B: 0.1 % trifluoroacetic acid in acetonitrile) at a flow rate of 1 mL/min. The molecular weight was measured by a SHIMADZU LCMS-2020 mass spectrometer. These data are provided in Figure S1.

### 2.2. Biolayer interferometry (BLI)

The binding of peptides to the SARS-CoV-2 spike RBD (40592-V08B-B, Sino Biological, Beijing, China) were measured by BLI (Octet Red 96, Sartorius, Göttingen, Germany). The biotinylated RBD was immobilized on streptavidin (SA) biosensors at 15 µg/mL. Peptides were prepared in PBS at concentrations of 50, 100, 200, 400, 600, and 800 nM. The signals corresponding to association and disassociation at 30 °C for 300 s each were recorded at a shaking speed of 1000 rpm. The data were processed using ForteBio Data Analysis 7.0 software. The equilibrium dissociation constant ( $K_D$ ) values were obtained by global fitting using a 1:1 fitting model.

### 2.3. Western blotting

A549 cells purchased from the Cell Bank of the Chinese Academy of Sciences (CAS, Shanghai, China) were seeded into a 6-well plate ( $1 \times 10^6$  cells/well) and cultured in Dulbecco's modified Eagle's medium (DMEM, Gibco, Thermo Fisher Scientific, Shanghai, China) containing 10 % fetal bovine serum (FBS, Gibco). SARS-CoV-2 S1 (20 µg/mL, 40591-V08H, Sino Biological) preincubated with LD-11, ED-10, or GK-7 (1, 10, and 50 µg/mL) for 15 min was added to the cells, followed by incubation at 37 °C for 1 h. The cells were then washed three times

with sterile PBS to remove dissociative SARS-CoV-2 S1 and lysed with RIPA lysis and extraction buffer (89900, Thermo Fisher Scientific). The amount of SARS-CoV-2 S1 attached to the cells was detected using an anti-spike rabbit polyclonal primary antibody (40591-T62, Sino Biological, 1:1000) and a goat anti-rabbit secondary antibody (A0208, Beyotime, Shanghai, China). As a reference, the amount of β-actin was detected using a rabbit monoclonal antibody (AF5003, Beyotime). The experiment was repeated three times on different days.

### 2.4. Immunofluorescence microscopy

A549 cells were cultured on sterile glass slides in a 12-well plate ( $2 \times 10^5$  cells/well). After washing with sterile PBS, the cells were exposed to 10 µg/mL SARS-CoV-2 S1 pretreated with 50 µg/mL GK-7 at 37 °C for 15 min. Coincubation was performed for another 1 h. SARS-CoV-2 S1 attached to the cell surface was stained using an anti-spike rabbit polyclonal primary antibody (40591-T62, Sino Biological, 1:200) and a goat antirabbit secondary antibody (Alexa Fluor 488, Invitrogen, Thermo Fisher Scientific). Cells in the sham group were treated with normal rabbit IgG (A7016, Beyotime, 1:200). Nuclei were stained with 4',6-diamidino-2-phenylindole dihydrochloride (DAPI, C1002, Beyotime). A Zeiss LSM 780 NLO confocal microscope was applied to observe the cells.

### 2.5. In vitro pseudovirion infection assay

Human embryonic kidney 293T cells transfected with human ACE2 (HEK-293T-hACE2) were seeded into a 96-well plate ( $5 \times 10^3$  cells/well) and cultured overnight. SARS-CoV-2 spike pseudovirions (20 µL,  $1.98 \times 10^7$  TU/mL) preincubated with increasing concentrations of GK-7 (0.39, 0.78, 1.56, 3.13, 6.25, 12.5, 25, 50, 75, and 100 µg/mL), LD-11 (0.78, 1.56, 3.13, 6.25, 12.5, 25, 50, 75, 100, and 200 µg/mL), or ACE2 (10108-H02H, Sino Biological, 0.005, 0.01, 0.02, 0.04, 0.08, 0.16, 0.31, 0.63, and 1.2 µg/mL) at 37 °C for 1 h were added to the cells, followed by 12 h of incubation. After removal of the pseudovirions, the cells were further cultured for 48 h. Pseudovirion infection was assessed by determining luciferase activity using a dual-luciferase reporter assay system (E1910, Promega, Beijing, China). This experiment was conducted in triplicate and repeated twice.

### 2.6. Molecular docking

Docking studies were carried out by Wecomput Technology (Beijing, China) using the Autodock Vina program [24]. The structure of the SARS-CoV-2 S1 RBD was extracted from a binding complex with ACE2 (PDB ID: 6M0J [22]). The protein was converted to a PDBQT file containing a protein structure with hydrogens in all polar residues. All ligand bonds were set as rotatable. All calculations for protein-fixed ligand-flexible docking were performed using the Lamarckian genetic algorithm (LGA). The docking site on the protein target was defined by establishing a grid box with the default grid spacing centered on the position of the active residues Gly446, Gln493, Gly496, Gln498, Thr500 and Gly502. The best conformation with the lowest binding energy was chosen for further MDS.

### 2.7. MDS

MDS was performed using AMBER16 [25]. The complex of GK-7 with the SARS-CoV-2 S1 RBD was neutralized by adding sodium/chlorine counterions and solvated in a cuboid box of TIP3P water molecules with solvent layers of 10 Å between the box edges and solute surface. AMBER FF14SB force fields were applied, and the SHAKE algorithm was used to restrict all covalent bonds involving hydrogen atoms with a time step of 2 fs. The particle mesh Ewald (PME) method was employed to treat long-range electrostatic interactions. For each solvated system, two minimization steps were performed before the heating step. The first

4000 minimization cycles were performed with all heavy atoms restrained at 50 kcal/(mol·Å<sup>2</sup>), whereas solvent molecules and hydrogen atoms were free to move. Then, nonrestrained minimization was carried out involving 2000 cycles of steepest descent minimization and 2000 cycles of conjugated gradient minimization. Afterward, the whole system was first heated from 0 to 300 K in 50 ps using Langevin dynamics at a constant volume and then equilibrated for 400 ps at a constant pressure of 1 atm. A weak constraint of 10 kcal/(mol·Å<sup>2</sup>) was used to restrain all the heavy atoms during the heating steps. Periodic boundary dynamics simulations were carried out for the whole system with a constant composition, pressure, and temperature (NPT) ensemble at a constant pressure of 1 atm and temperature of 300 K in the production step. In the production phase, a 100 ns simulation was carried out. The binding free energy of the complex was calculated using the molecular mechanics with Poisson–Boltzmann and surface area solvation (MM-PBSA) method.

## 2.8. Toxicity evaluation

Human umbilical vein endothelial cells (HUVECs) obtained from the CAS were seeded into a 96-well plate ( $5 \times 10^3$  cells/well). After adherence, the cells were exposed to increasing concentrations of GK-7 (3.13, 6.25, 12.5, 25, 50, 100, and 200 µg/mL) at 37 °C for 24 h. The viability of HUVECs was measured using a Cell Counting Kit-8 (CCK-8; Dojindo, Shanghai, China). A hemolytic test was performed as we recently described [26]. Briefly, mouse red blood cells (300 µL) diluted in 0.9% NaCl solution were incubated with 1.2 mL of GK-7 (25, 50, 100, and 200 µg/mL) at 37 °C for 2 h. The absorbance of the supernatant collected by centrifugation at 10,000 ×g for 5 min was determined at 405 nm using a microplate reader.

The *in vivo* toxicity of GK-7 was evaluated with mouse experiments approved by the Animal Experimental Ethics Committee of the Third Military Medical University. Mice were cared for and treated in accordance with the National Institutes of Health (NIH) Guidelines for the

Care and Use of Laboratory Animals (NIH publication no. 85e23, rev. 1985). Twenty 8-week-old female BALB/c mice (18–22 g) were randomly divided into 2 groups (n = 10). GK-7 was intranasally administered at a single dose of 2.5 mg/kg. Mouse tail venous blood was analyzed on a Sysmex XT-2000i fully automatic hematology analyzer (Kobe, Japan) at 7 days after injection. The mice were sacrificed on day 7. Hematoxylin and eosin (HE) staining and an Olympus DX51 optical microscope (Tokyo, Japan) were applied to observe the pathological changes in major organs. The mice in the sham group were treated with sterile PBS.

## 2.9. Statistical analysis

The SPSS 25.0 software was employed to determine the significance of differences (*P*) using one-way ANOVA with the least significant difference (LSD) multiple comparison test and Student's *t*-test. *P* < 0.05 was considered statistically significant.

## 3. Results

### 3.1. Peptide design and synthesis

Twenty critical residues (CRs) in ACE2 bind to SARS-CoV-2 RBD within a distance of 4 Å [22]. More than half of the CRs are located in the N-terminal helix of ACE2 (Fig. 1). We focused on residues Glu23 to Ala46 and designed five short derivatives, *i.e.*, EQ-10, KT-11, LD-11, NH-11, and ED-10, which contained 4–6 CRs. Because four CRs, Lys353, Gly354, Asp355, and Arg357, in the linker between β3 and β4 of ACE2 also contribute to the interaction with the SARS-CoV-2 spike RBD, we further extracted residues ranging from Gly352 to Ile358 and obtained GK-7. All the peptides were prepared by solid-phase chemical synthesis. The determined molecular weights of the peptides matched closely with their theoretical values (Figure S1), indicative of successful synthesis.

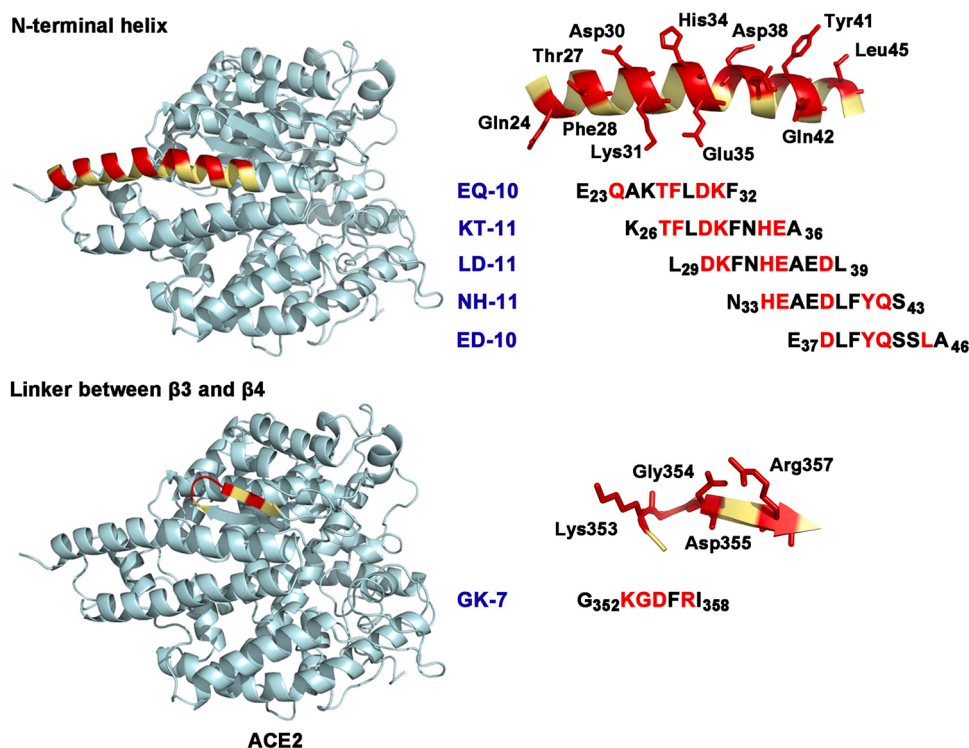


**Fig. 1.** Diagram depicting the design of short peptides derived from ACE2. The extracellular domain of ACE2 is presented as ribbon structure. EQ-10, KT-11, LD-11, NH-11, and ED-10 are derived from the N-terminal helix of ACE2. GK-7 is extracted from the linker between β3 and β4 of ACE2. The critical residues contributing to the interaction of ACE2 with SARS-CoV-2 spike in the peptides are shown in sticks and colored red.

### 3.2. Bindings of peptides to the SARS-CoV-2 spike RBD

The interactions of peptides at different concentrations with the biotinylated SARS-CoV-2 spike RBD loaded on SA biosensors were determined by BLI. EQ-10 possesses 5 CRs and bound to the RBD at 47.8 nM, comparable with that of ED-10 (45.9 nM, 4 CRs) associated with the RBD (Fig. 2). No signals were detected for KT-11, although it has 6 CRs. LD-11 (5 CRs) and GK-7 (4 CRs) bound to the RBD at 35.2 nM and 25.1 nM, respectively, which were over 40-fold lower affinities than that of NH-11 (1.53  $\mu$ M, 5 CRs). Notably, GK-7 was the simplest peptide but was the most potent binder for the SARS-CoV-2 spike RBD.

### 3.3. Inhibition of SARS-CoV-2 S1 attachment by GK-7

To evaluate the effect of peptide binding on SARS-CoV-2 S1 attachment, we performed a cell experiment in which human alveolar epithelial A549 cells were exposed to 20  $\mu$ g/mL SARS-CoV-2 S1 pre-treated with LD-11, ED-10, or GK-7. After 1 h of coincubation, the amount of SARS-CoV-2 S1 adhered to A549 cells was determined by Western blotting. Consistent with the discrepancy in RBD association, GK-7 was more efficient than LD-11 and ED-10 in decreasing S1 attachment at 50  $\mu$ g/mL (Fig. 3A). Moreover, GK-7 suppression occurred in a dose-dependent manner (Fig. 3B). Confocal microscopy supported

that SARS-CoV-2 S1 generally adhered to the surface of A549 cells in the absence of GK-7 (Fig. 3C). However, when SARS-CoV-2 S1 was pre-treated with 50  $\mu$ g/mL GK-7, protein attachment was dramatically reduced (Figure S2).

### 3.4. Inhibition of SARS-CoV-2 spike pseudovirion infection by GK-7

SARS-CoV-2 spike pseudovirions equipped with a luciferase reporter system were employed to infect HEK-293T-hACE2 cells in the presence of increasing concentrations of peptides. As shown in Fig. 4A, GK-7 exerted a dose-dependent antiviral effect. The half-maximal inhibitory concentration ( $IC_{50}$ ) of GK-7 was 2.96  $\mu$ g/mL, 4.12-fold lower than that of LD-11 (12.2  $\mu$ g/mL, Fig. 4B), which was in line with the superiority of GK-7 to LD-11 in binding to the SARS-CoV-2 spike RBD and decreasing S1 attachment to A549 cells. Nevertheless, compared with the prototype ACE2 that had an  $IC_{50}$  as low as 0.067  $\mu$ g/mL (Fig. 4C), GK-7 was less efficient in suppressing the pseudovirion infection.

### 3.5. Blockade of the binding interface of SARS-CoV-2 spike RBD by GK-7

To gain insights into the binding of GK-7 to the RBD, we performed molecular docking followed by an all-atom MDS. As shown in Fig. 5A, the system achieved equilibrium within the simulation time, and the

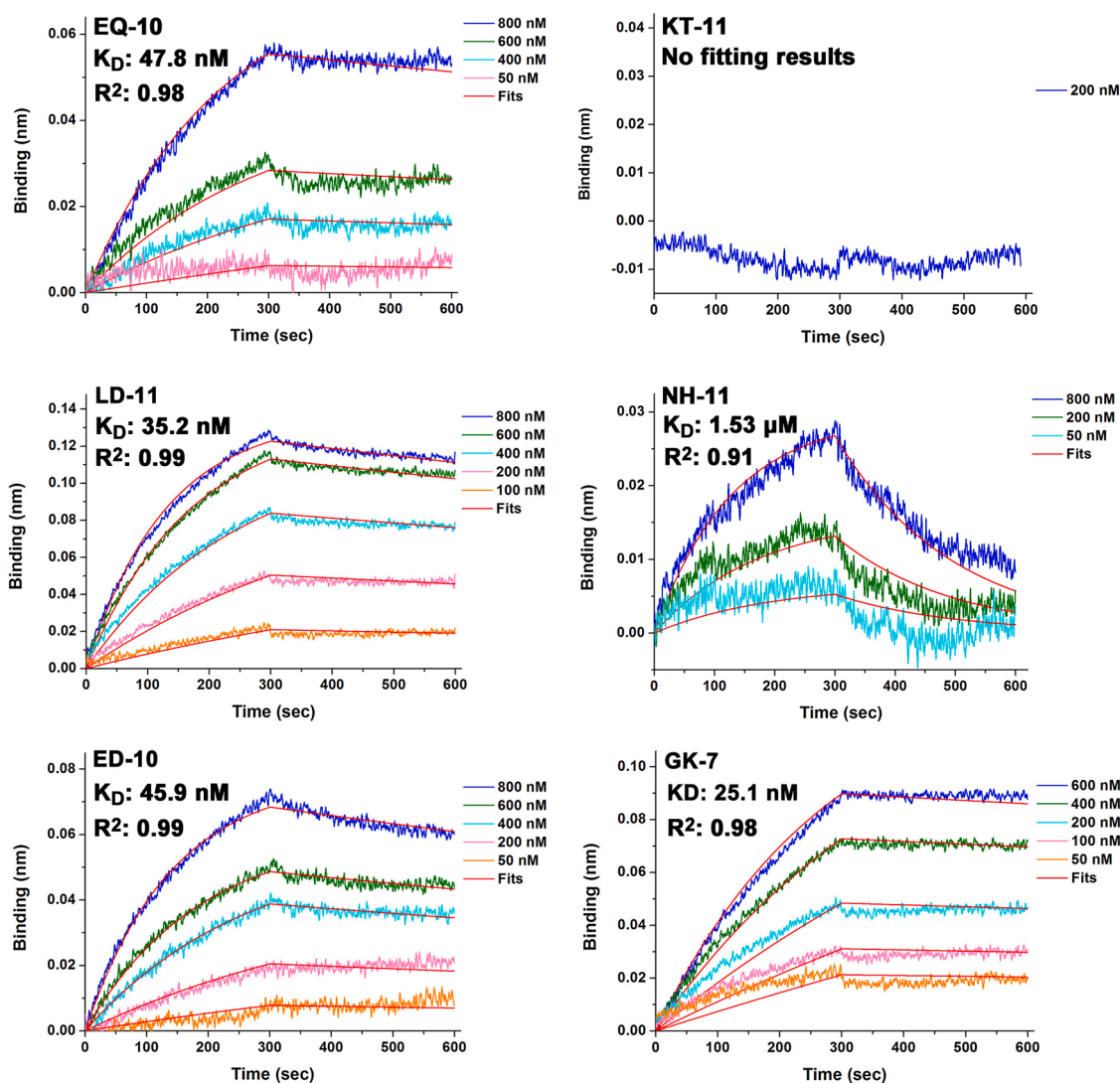
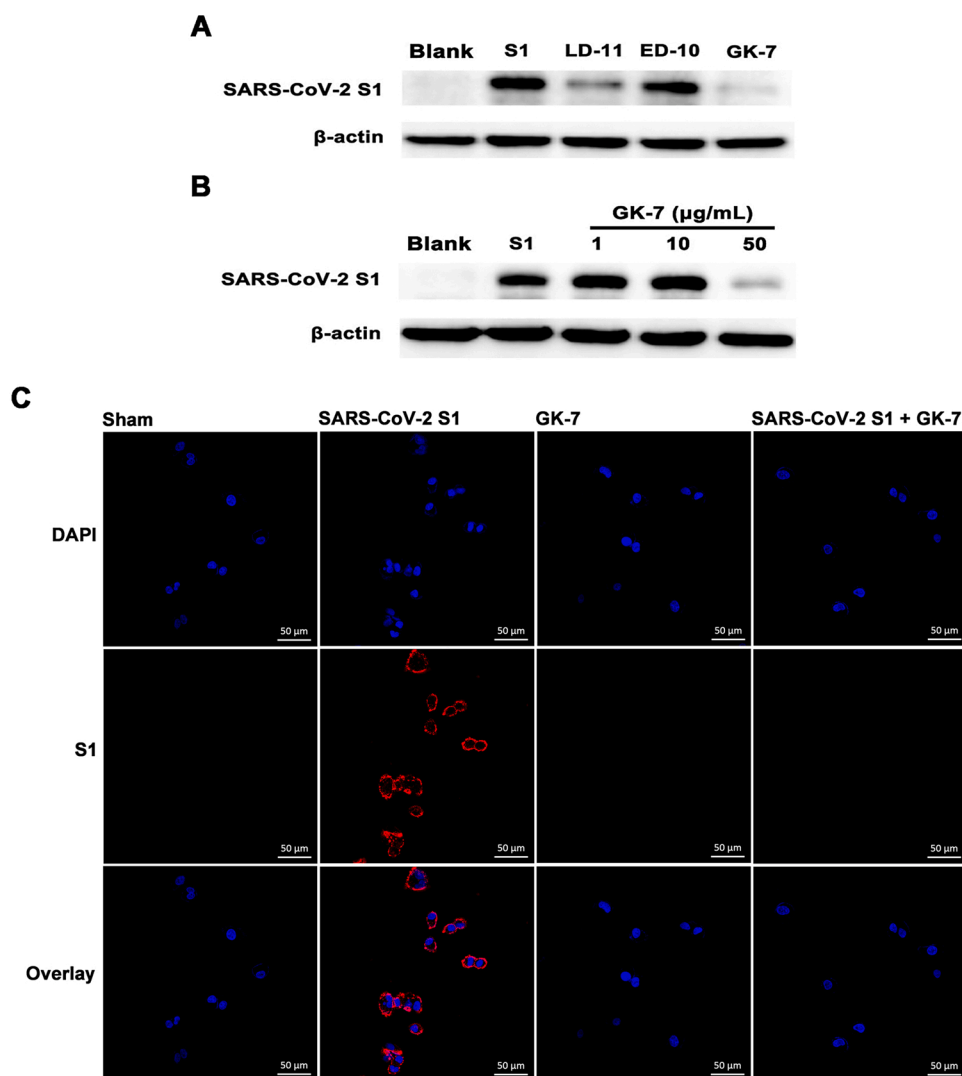
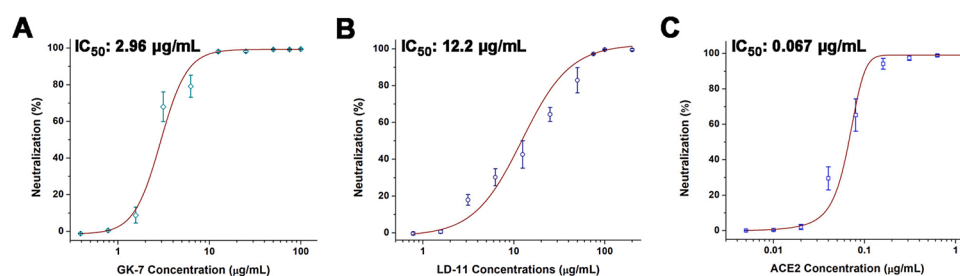


Fig. 2. Binding kinetics for peptides and the SARS-CoV-2 spike RBD loaded on SA biosensors. The running times for association and disassociation are both 300 s. The binding data were processed by interstep correction and Savitzky-Golay filtering. The fitted curves are colored red.



**Fig. 3.** Inhibitory effects of GK-7 on SARS-CoV-2 S1 adherence to cells. (A) Western blotting detection of SARS-CoV-2 S1 binding to A549 cells in the absence and presence of 50 µg/mL LD-11, ED-10, and GK-7. β-actin was used as the reference. (B) Dose-dependent suppression of GK-7 on SARS-CoV-2 S1 binding to A549 cells. (C) Immunofluorescence microscopy revealing the protective effect of GK-7 on A549 cells exposed to SARS-CoV-2 S1 (red). Nuclei were stained with DAPI (blue). The scale bar indicates 50 µm.



**Fig. 4.** Antiviral action of GK-7 against SARS-CoV-2 spike pseudovirion infection. (A) Dose-dependent antiviral activity of GK-7, (B) LD-11, and (C) ACE2 against pseudovirions. Results are shown as mean  $\pm$  standard deviation (SD). The fitted curves obtained by nonlinear regression are in burgundy.

root mean square deviations (RMSDs) of the backbones of GK-7 and the SARS-CoV-2 spike RBD are less than 3.5 Å. The variations in the complex structure at different simulation times are shown in Movie S1. The final conformation revealed that the oxygen atom of the backbone of Gly496 in the RBD, regarded as a hydrogen bond acceptor, formed one hydrogen bond with a carbon atom of the side chain of Lys2 in GK-7; the oxygen atom of the hydroxyl of Thr500 in the RBD, regarded as a hydrogen bond donor, formed one hydrogen bond with the oxygen atom of the carboxyl of Asp4 in GK-7; and the nitrogen atom of the backbone of Gly502 in the RBD, regarded as hydrogen bond donor, formed one hydrogen bond with the oxygen atom of the backbone of Lys2 in GK-7 (Fig. 5B). Driven

by intermolecular interactions, principally van der Waals forces, GK-7 bound to the SARS-CoV-2 spike RBD with a binding free energy of -52.23 kcal/mol.

### 3.6. Evaluation of GK-7 toxicity *in vitro* and *in vivo*

To evaluate the cytotoxicity of GK-7, we incubated HUVECs with increasing concentrations of the peptide. GK-7 did not affect cell survival after 24 h at doses up to 200 µg/mL (Fig. 6A), which was approximately 68-fold higher than the  $IC_{50}$  value of GK-7 in inhibiting SARS-CoV-2 spike pseudovirion infection. Additionally, GK-7 exhibited negligible

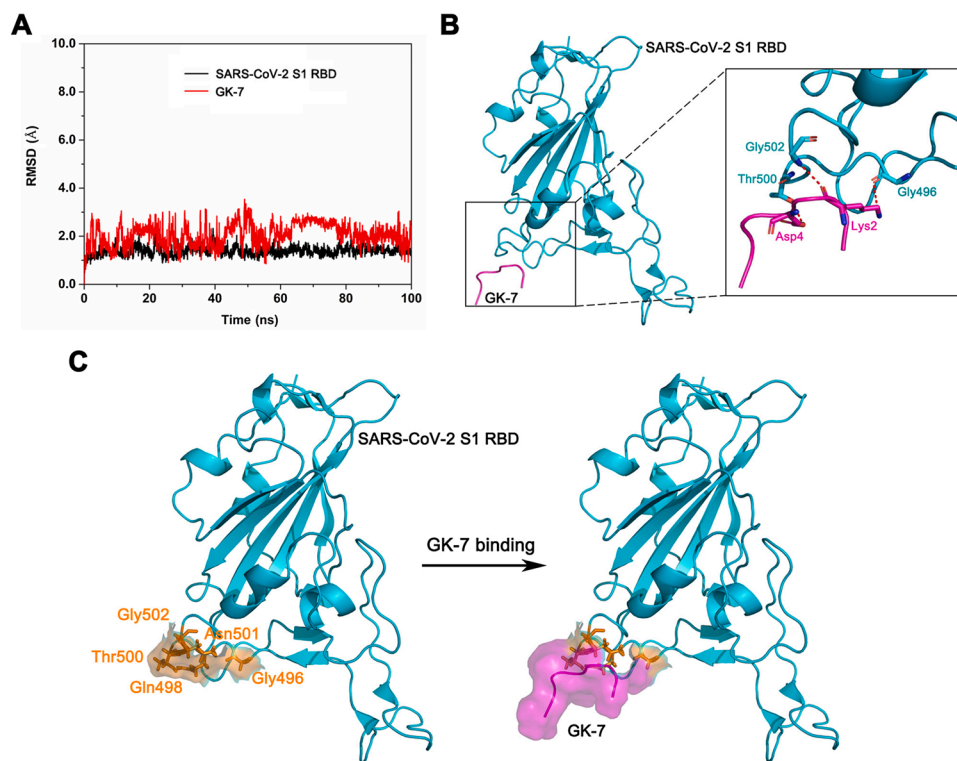


**Fig. 5.** Molecular dynamics simulation revealing the blockade of the SARS-CoV-2 spike RBD by GK-7. (A) The RMSDs of the backbones of GK-7 and the RBD. (B) Complex structure of GK-7 with the RBD. GK-7 is colored magenta. The RBD is in cyan. The residues contributing to the intermolecular interaction are shown in sticks. The red dashes represent hydrogen bonds. (C) Stereoview of the cloak of GK-7 on the RBD. The residues in the RBD cloaked by GK-7 (magenta) are colored orange.

hemolysis (Fig. 6B), indicative of biosafety *in vitro*. For *in vivo* assessment, BALB/c mice were given 2.5 mg/kg GK-7 (1 mg/mL, 50  $\mu$ L) by intranasal administration. The major organs, including the heart, liver, spleen, lungs, and kidneys, were obtained 7 days after the initial peptide delivery. GK-7 administration had minor effects on the organ index (Fig. 6C); the RBC, WBC, and platelet counts (Fig. 6D–F) in the blood; and the alanine aminotransferase (ALT), aspartate aminotransferase (AST), blood urea and creatinine contents (Figure S3). HE staining revealed no pathological changes in the tissues (Fig. 6G). These data indicated nontoxicity *in vivo* and laid a solid foundation for the topical application of GK-7 as a peptide antagonist against SARS-CoV-2.

#### 4. Discussion

The ongoing COVID-19 epidemic worldwide necessitates effective solutions. Currently, SARS-CoV-2 vaccines have attracted great attention. Despite the efficient protection against SARS-CoV-2 infection, vaccinated individuals may be susceptible to the highly pathogenic virus, particularly under conditions of high exposure risk [27]. Continuous viral variation also challenges the efficacy of current vaccines [28]. Accordingly, the development of antiviral agents against SARS-CoV-2 is still urgently needed. Among all the candidates, peptide antagonists, which can be divided into attachment inhibitors, fusion and entry inhibitors, enzyme inhibitors, replication inhibitors, and peptides with direct and indirect effects on SARS-CoV-2 [12,29], hold promise for COVID-19 treatment [20].

Because the interaction between the viral spike RBD and host ACE2 is the initial step of SARS-CoV-2 infection, attachment inhibitors blocking the RBD are expected to achieve direct viral inhibition. These peptides can be derived from natural sources and rationally designed. Griffithsin (GRFT), a lectin peptide isolated from the red alga *Griffithsia sp* [30], and human cathelicidin LL37 represent natural products with the capabilities of binding to the RBD and blocking SARS-CoV-2 spike pseudovirion infection [23]. Nevertheless, these peptides are composed of more than 30 amino acids and have high preparation costs. Alternatively, peptide inhibitors designed by combining the CRs in the binding interface can be

short and facile for synthesis [31]. For instance, the hexapeptide YK-6 is part of the SARS-CoV RBD with dominant CRs for ACE2 attachment; it inhibits SARS-CoV infection by cloaking ACE2 [32]. The heptapeptide GK-7 in our study contains CRs of ACE2 and bound to the RBD, which blocked SARS-CoV-2 S1 adherence and suppressed pseudovirion infection with an  $IC_{50}$  of 2.96  $\mu$ g/mL, approximately 44-fold higher than that of ACE2 but 1.6-fold lower than that of LL37 (4.74  $\mu$ g/mL) [23].

Recently, several spike-targeting ACE2-derived peptides (SAPs) were designed and found with higher  $IC_{50}$  values than GK-7 in suppressing SARS-CoV-2 spike pseudovirion infection [31]. However, because the exposure duration of pseudovirion to HEK-293T-hACE2 cells in the present study was 12 h, much less than that in the SAPs study (48 h), there is no comparability in the antiviral actions between GK-7 and SAPs. Interestingly, we noticed that SAP4, a peptide with only one more Leu in the sequence relative to GK-7, was a weak viral inhibitor [31]. Our data supported that SAP4 was inefficient to inhibit pseudovirion infection (Figure S4). Comparatively, SAP4 was inferior to GK-7 in protecting cells from viral invasion, possibly due to the alteration of active residues distribution in the solvent-accessible surface caused by C-terminal addition of hydrophobic Leu [33].

GK-7 contains 4 CRs and bound to the RBD at 25.1 nM, which was a 3.2-fold higher affinity than that of ACE2 interacting with the RBD [23]. KT-11 has 6 CRs but fails to bind to the RBD. The noncorrelation of the binding affinities to the number of CRs is primarily due to conformational alterations as well. The N-terminal helix (Thr22 to Asn49) was shown to change to a random coil in solution after extraction from ACE2 [34]. Since conformation determines the function of proteins, the linear peptide was found to be almost inactive for binding to the SARS-CoV-2 spike RBD and suppressing viral infection. However, when the helicity was recovered by double stapling, the constrained peptide was found to exert a good inhibitory effect [34]. It is plausible that maintaining helical properties by introducing stapled amino acids or disulfide bonds could be instrumental for enhancing the binding ability and antiviral action of KT-11 [35,36]. For GK-7, a short peptide designed by extracting residues located in the flexible linker of ACE2, its conformation is closer to the natural state than that of peptides derived from

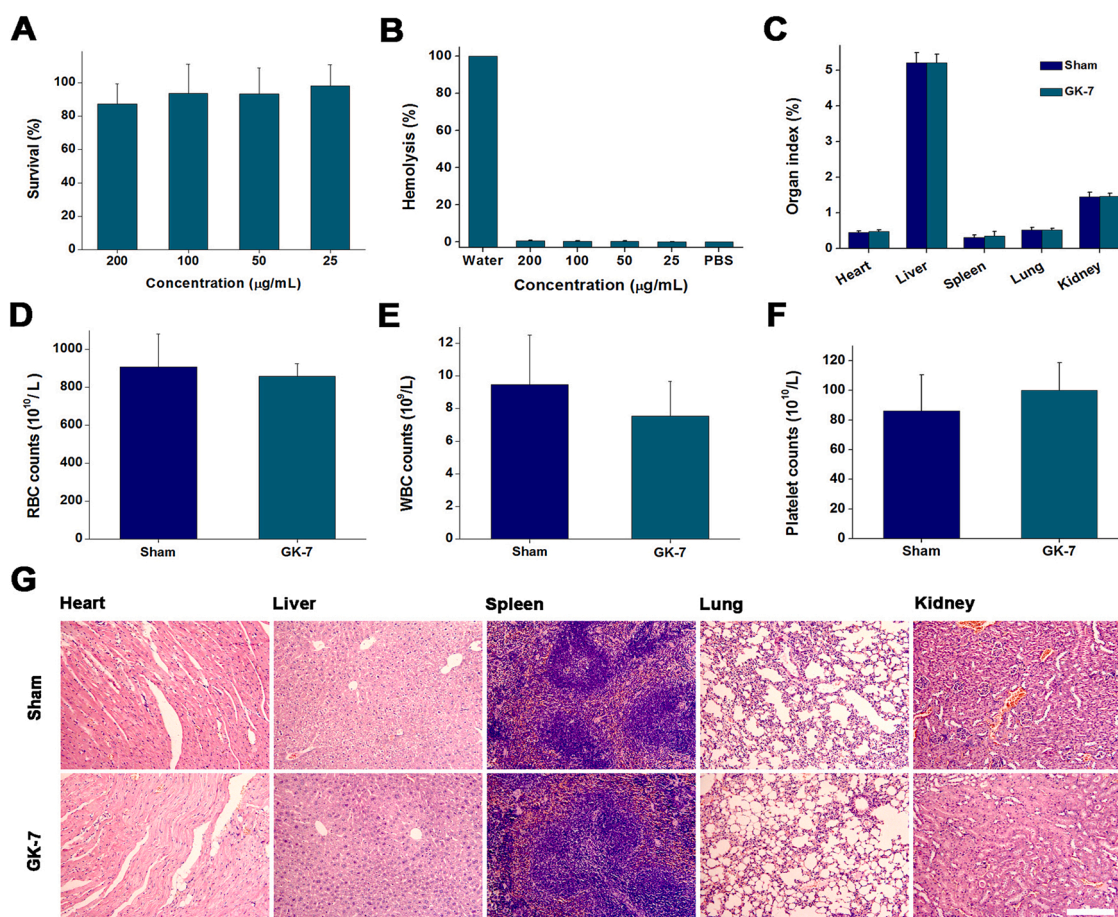


**Fig. 6.** Toxicity analysis of GK-7 *in vitro* and *in vivo*. (A) Survival of HUVECs exposed to different concentrations of GK-7 for 24 h. The results are shown as the means  $\pm$  SDs. (B) Hemolysis of different doses of GK-7. The results are shown as the means  $\pm$  SDs. Sterile water was employed as a positive control. (C) Organ indexes of mice treated with PBS (sham) and GK-7. The results are shown as the means  $\pm$  SDs. (D) Counts of RBCs, (E) WBCs, and (F) platelets in mouse blood at 7 days post injection of GK-7. The results are presented as the means  $\pm$  SDs. (G) HE staining of the organs of mice treated with sterile PBS (sham) and GK-7. The scale bar indicates 200  $\mu$ m.

the helix, which supports the efficacies of the CRs in GK-7, particularly for the binding "hotspot" Lys353 [37].

Lys353, a site corresponds to Lys2 in GK-7, is highly conserved in mammalian ACE2 [37]. Because 2 of the 3 hydrogen bonds by which GK-7 bound to the SARS-CoV-2 spike RBD were donated by Lys2, this site was also a binding "hotspot" in GK-7. Previous studies have demonstrated that mutations to SARS-CoV-2 spike Gly502 abolish the binding of the RBD to ACE2 due to steric clashes [38]. LL37 inhibits SARS-CoV-2 S1 adherence by blocking 5 CRs in the RBD, including Thr500 and Asn501 [23]. Additionally, the miniprotein inhibitor LCB2 bound to the SARS-CoV-2 spike RBD via 35 binding sites, 16 of which encompassed Gly496, Gln498, Thr500, Asn501, and Gly502 and overlapped with the CRs of the RBD involved in ACE2 binding [19]. Our MDS results showed that GK-7 bound to Gly496, Thr500, and Gly502, 3 of the 18 CRs in the RBD [22]. Exposure of Gln498 and Asn501 was also cloaked by GK-7 (Fig. 5C). These findings help to explain the mechanism by which GK-7 blocks RBD binding.

In summary, in the present study, we designed and prepared a peptide inhibitor of SARS-CoV-2 based on the ligand-binding domain of the viral receptor ACE2. The peptide termed GK-7 is composed of 7 amino acids and contained 4 CRs contributing to the stabilization of the binding interface of the SARS-CoV-2 spike RBD with ACE2. Inspiringly, GK-7 bound to the RBD at high affinity and exerted inhibitory effects on spike attachment to sensitive cells as well as on the invasion of SARS-CoV-2 spike pseudovirions. GK-7 is part of a natural protein and has the advantage of low immunogenicity compared with that of *de novo*

designed inhibitors. Considering that SARS-CoV-2 usually invades the human body via the respiratory pathway, topical application of GK-7 to the nose and lung by intranasal administration or aerosolization could be beneficial for curbing viral infection. GK-7 is an easy-to-produce peptide inhibitor of SARS-CoV-2 attachment and has good prospects for drug development.

#### CRediT authorship contribution statement

This study demonstrates a useful peptide antagonist that can be easily prepared for curbing SARS-CoV-2, which is a promising drug candidate to treat COVID-19. We believe that the findings are relevant to the scope of *Peptides* and will be of interest to its readership. The complete author list is: S. Han, G. Zhao, Z. Wei, Y. Chen, J. Zhao, Y. He, Y. J. He, J. Gao, S. Chen, C. Du, T. Wang, W. Sun, Y. Huang, C. Wang, and J. Wang.

S. Han, G. Zhao, and Z. Wei contributed equally to this paper. S. Han: Data curation, Investigation, Visualization, Funding acquisition. G. Zhao: Data curation, Investigation, Visualization. Z. Wei: Investigation, Visualization. Y. Chen: Investigation, Methodology. J. Zhao and Y. He: Methodology, Formal analysis. Y. J. He, J. Gao, S. Chen, and C. Du: Validation, Software. T. Wang: Supervision. W. Sun and Y. Huang: Methodology, Resources. C. Wang: Conceptualization, Funding acquisition, Project administration, Writing - original draft. J. Wang: Funding acquisition, Project administration, Writing - review & editing.

## Declaration of Competing Interest

The authors declare the following competing financial interest (s): Cheng Wang and Junping Wang have filed a patent application for the peptide.

## Acknowledgments

This work was supported by the Natural Science Fundation of Chongqing City (cstc2019jcyj-msxmX0011) and the grants from the National Natural Science Foundation of China (Nos. 81725019 and 82003395).

## Appendix A. Supplementary data

Supplementary material related to this article can be found, in the online version, at doi:<https://doi.org/10.1016/j.peptides.2021.170638>.

## References

- Coronaviridae Study Group of the International Committee on Taxonomy of Viruses, The species severe acute respiratory syndrome-related coronavirus: classifying 2019-nCoV and naming it SARS-CoV-2, *Nat. Microbiol.* 5 (4) (2020) 536–544.
- B.B.O. Munnink, R.S. Sikkema, D.F. Nieuwenhuijse, R.J. Molenaar, E. Munger, R. Molenkamp, et al., Transmission of SARS-CoV-2 on mink farms between humans and mink and back to humans, *Science* 37 (2021) 172–177.
- A.J. Vivanti, C. Vauloup-Fellous, S. Prevot, V. Zupan, C. Suffee, J. Do Cao, et al., Transplacental transmission of SARS-CoV-2 infection, *Nat. Commun.* 11 (2020) 3572.
- E. Petersen, M. Koopmans, U. Go, D.H. Hamer, N. Petrosillo, F. Castelli, et al., Comparing SARS-CoV-2 with SARS-CoV and influenza pandemics, *Lancet Infect. Dis.* 20 (2020) E238–E244.
- D. Wang, B. Hu, C. Hu, F. Zhu, X. Liu, J. Zhang, et al., Clinical characteristics of 138 hospitalized patients with 2019 novel coronavirus-infected pneumonia in Wuhan, China, *JAMA* 323 (11) (2020) 1061–1069.
- W. Guan, Z. Ni, Y. Hu, W. Liang, C. Ou, J. He, et al., Clinical characteristics of coronavirus disease 2019 in China, *N. Engl. J. Med.* 382 (18) (2020) 1708–1720.
- Z. Xu, L. Shi, Y. Wang, J. Zhang, L. Huang, C. Zhang, et al., Pathological findings of COVID-19 associated with acute respiratory distress syndrome, *Lancet Respir. Med.* 8 (2020) 420–422.
- T. Chen, D. Wu, H. Chen, W. Yan, D. Yang, G. Chen, et al., Clinical characteristics of 113 deceased patients with coronavirus disease 2019: retrospective study, *BMJ* 368 (2020) m1091.
- A.C. Walls, Y.J. Park, M.A. Tortorici, A. Wall, A.T. McGuire, D. Velesler, Structure, function, and antigenicity of the SARS-CoV-2 spike glycoprotein, *Cell* 181 (2020), 281–292 e6.
- N. Dong, X. Yang, L. Ye, K. Chen, W. Chan, M. Yang, et al., Genomic and protein structure modelling analysis depicts the origin and pathogenicity of 2019-nCoV, a new coronavirus which caused a pneumonia outbreak in Wuhan, China, *F1000Research* 9 (2020) 121.
- X. Xu, P. Chen, J. Wang, J. Feng, H. Zhou, X. Li, et al., Evolution of the novel coronavirus from the ongoing Wuhan outbreak and modeling of its spike protein for risk of human transmission, *Sci. China Life Sci.* 63 (3) (2020) 457–460.
- C. Wang, S. Wang, D. Li, D.Q. Wei, J. Zhao, J. Wang, Human intestinal defensin 5 inhibits SARS-CoV-2 invasion by cloaking ACE2, *Gastroenterology* 159 (2020), 1145–1147 e4.
- M. Hoffmann, H. Kleine-Weber, S. Schroeder, N. Krüger, T. Herrler, S. Erichsen, et al., SARS-CoV-2 cell entry depends on ACE2 and TMPRSS2 and is blocked by a clinically proven protease inhibitor, *Cell* 181 (2020), 271–280 e8.
- C.G.K. Ziegler, S.J. Allon, S.K. Nyquist, I.M. Mbanjo, V.N. Miao, C.N. Tzouanas, et al., SARS-CoV-2 receptor ACE2 is an interferon-stimulated gene in human airway epithelial cells and is detected in specific cell subsets across tissues, *Cell* 181 (2020), 1016–1035 e19.
- Y.J. Hou, K. Okuda, C.E. Edwards, D.R. Martinez, T. Asakura, K.H. Dinnon, et al., SARS-CoV-2 reverse genetics reveals a variable infection gradient in the respiratory tract, *Cell* 182 (2020), 429–446 e14.
- S. Pinkert, B. Dieringer, S. Diedrich, H. Zeichhardt, J. Kurreck, H. Fechner, Soluble coxsackie- and adenovirus receptor (sCAR-Fc); a highly efficient compound against laboratory and clinical strains of coxsackie-B-virus, *Antiviral Res.* 136 (2016) 1–8.
- V. Monteil, H. Kwon, P. Prado, A. Hagekruys, R.A. Wimmer, M. Stahl, et al., Inhibition of SARS-CoV-2 infections in engineered human tissues using clinical-grade soluble human ACE2, *Cell* 181 (2020), 905–913 e7.
- D. Pinto, Y.J. Park, M. Beltramello, A.C. Walls, M.A. Tortorici, S. Bianchi, et al., Cross-neutralization of SARS-CoV-2 by a human monoclonal SARS-CoV antibody, *Nature* 583 (2020) 290–295.
- L. Cao, I. Greshnik, B. Coventry, J.B. Case, L. Miller, L. Kozodoy, et al., De novo design of picomolar SARS-CoV-2 miniprotein inhibitors, *Science* 370 (2020) 426–431.
- D. Schütz, Y.B. Ruiz-Blanco, J. Münch, F. Kirchhoff, E. Sanchez-Garcia, J.A. Müller, Peptide and peptide-based inhibitors of SARS-CoV-2 entry, *Adv. Drug Deliv. Rev.* 167 (2020) 47–65.
- P. Karoyan, V. Vieillard, L. Gómez-Morales, E. Odile, A. Guihot, C.-E. Luyt, et al., Human ACE2 peptide-mimics block SARS-CoV-2 pulmonary cells infection, *Commun. Biol.* 4 (2021) 197.
- J. Lan, J. Ge, J. Yu, S. Shan, H. Zhou, S. Fan, et al., Structure of the SARS-CoV-2 spike receptor-binding domain bound to the ACE2 receptor, *Nature* 581 (2020) 215–220.
- C. Wang, S. Wang, D. Li, P. Chen, S. Han, G. Zhao, et al., Human cathelicidin inhibits SARS-CoV-2 infection: killing two birds with one stone, *ACS Infect. Dis.* 7 (6) (2021) 1545–1554.
- O. Trott, A.J. Olson, AutoDock Vina: improving the speed and accuracy of docking with a new scoring function, efficient optimization, and multithreading, *J. Comput. Chem.* 31 (2010) 455–461.
- D.A. Case, T.E. Cheatham 3rd, T. Darden, H. Gohlke, R. Luo, K.M. Merz Jr., et al., The Amber biomolecular simulation programs, *J. Comput. Chem.* 26 (2005) 1668–1688.
- C. Wang, S. Wang, Y. Chen, J. Zhao, S. Han, G. Zhao, et al., Membrane nanoparticles derived from ACE2-rich cells block SARS-CoV-2 infection, *ACS Nano* 15 (2021) 6340–6351.
- C. Ma, S. Xu, Y. Yao, P. Yu, Y. Xu, R. Wu, et al., Mild breakthrough infection in a healthcare professional working in the isolation area of a hospital designated for treating COVID-19 patients -Shaanxi Province, China, March, 2021, *China CDC Weekly* 3 (2021) 397–400.
- W.G. dos Santos, Impact of virus genetic variability and host immunity for the success of COVID-19 vaccines, *Biomed. Pharmacother.* 136 (2021), 111272.
- H. Heydari, R. Golmohammadi, R. Mirnejad, H. Tebyanian, M. Fasihi-Ramandi, M. Moosazadeh Moghaddam, Antiviral peptides against Coronaviridae family: a review, *Peptides* 139 (2021), 170526.
- Y. Cai, W. Xu, C. Gu, X. Cai, D. Qu, L. Lu, et al., Griffithsin with a broad-spectrum antiviral activity by binding glycans in viral glycoprotein exhibits strong synergistic effect in combination with a pan-coronavirus fusion inhibitor targeting SARS-CoV-2 spike S2 subunit, *Virology* 535 (2020) 857–860.
- R.C. Larue, E. Xing, A.D. Kenney, Y. Zhang, J.A. Tuazon, J. Li, et al., Rationally designed ACE2-derived peptides inhibit SARS-CoV-2, *Bioconjug. Chem.* 32 (2021) 215–223.
- A.W. Struck, M. Axmann, S. Pfefferle, C. Drosten, B. Meyer, A hexapeptide of the receptor-binding domain of SARS corona virus spike protein blocks viral entry into host cells via the human receptor ACE2, *Antiviral Res.* 94 (2012) 288–296.
- G. Zou, E. de Leeuw, C. Li, M. Pazgier, C. Li, P. Zeng, et al., Toward understanding the cationicity of defensins: Arg and Lys versus their noncoded analogs, *J. Biol. Chem.* 282 (2007) 19653–19665.
- F. Curreli, S.M.B. Victor, S. Ahmed, A. Drelich, X. Tong, Tseng C-TK, et al., Stapled peptides based on human angiotensin-converting enzyme 2 (ACE2) potently inhibit SARS-CoV-2 infection *in vitro*, *mBio* 11 (2020) e02451-20.
- R. Mouratada, H.D. Herce, D.J. Yin, J.A. Morocco, T.E. Wales, J.R. Engen, et al., Design of stapled antimicrobial peptides that are stable, nontoxic and kill antibiotic-resistant bacteria in mice, *Nat. Biotechnol.* 37 (2019) 1186–1197.
- C. Wang, G. Zhao, S. Wang, Y. Chen, Y. Gong, S. Chen, et al., A simplified derivative of human defensin 5 with potent and efficient activity against multidrug-resistant *Acinetobacter baumannii*, *Antimicrob. Agents Chemother.* 62 (2018) e01504-17.
- J. Shang, G. Ye, K. Shi, Y. Wan, C. Luo, H. Aihara, et al., Structural basis of receptor recognition by SARS-CoV-2, *Nature* 581 (2020) 221–224.
- T.N. Starr, A.J. Greaney, S.K. Hilton, D. Ellis, K.H.D. Crawford, A.S. Dingens, et al., Deep mutational scanning of SARS-CoV-2 receptor binding domain reveals constraints on folding and ACE2 binding, *Cell* 182 (2020), 1295–1310 e20.